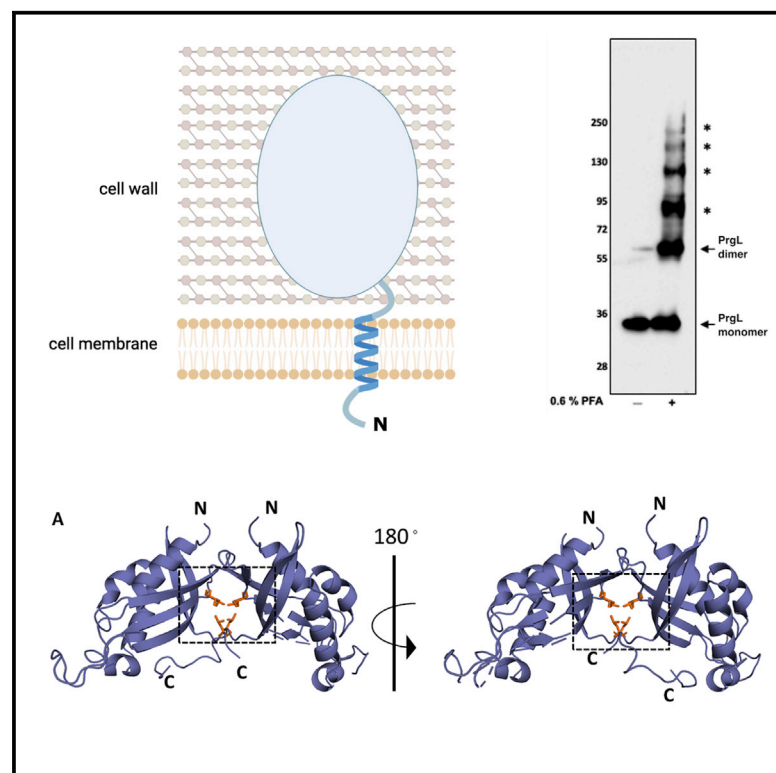# Structure of the enterococcal T4SS protein PrgL reveals unique dimerization interface in the VirB8 protein family

Graphical abstract

Authors

Franziska Jäger, Anaïs Lamy, Wei-Sheng Sun, Nina Guerini, Ronnie P-A Berntsson

Correspondence

ronnie.berntsson@umu.se

In brief

Jäger et al. use X-ray crystallography to determine the structure of the VirB8-like protein PrgL from *Enterococcus faecalis*. PrgL has an unusual dimer interface that is important for both higher oligomerization and the *in vivo* function of the pCF10 type 4 secretion system.

Highlights

- Structure of pCF10 PrgL

- PrgL forms dodecamers through its soluble domain

- Dimer interface is needed for *in vivo* function

CelPress

Article

Structure of the enterococcal T4SS protein PrgL reveals unique dimerization interface in the VirB8 protein family

Franziska Jäger,[1] Anaïs Lamy,[1,2] Wei-Sheng Sun,[1,2] Nina Guerini,[1] and Ronnie P-A Berntsson[1,2,3,*]
[1]Department of Medical Biochemistry and Biophysics, Umeå University, 90187, Umeå, Sweden
[2]Wallenberg Centre for Molecular Medicine, Umeå University, Umeå, Sweden
[3]Lead contact
*Correspondence: ronnie.berntsson@umu.se
https://doi.org/10.1016/j.str.2022.03.013

SUMMARY

Multidrug-resistant bacteria pose serious problems in hospital-acquired infections (HAIs). Most antibiotic resistance genes are acquired via conjugative gene transfer, mediated by type 4 secretion systems (T4SS). Although most multidrug-resistant bacteria responsible for HAIs are of Gram-positive origin, with enterococci being major contributors, mostly Gram-negative T4SSs have been characterized. Here, we describe the structure and organization of PrgL, a core protein of the T4SS channel, encoded by the pCF10 plasmid from *Enterococcus faecalis*. The structure of PrgL displays similarity to VirB8 proteins of Gram-negative T4SSs. *In vitro* experiments show that the soluble domain alone is enough to drive both dimerization and dodecamerization, with a dimerization interface that differs from all other known VirB8-like proteins. *In vivo* experiments verify the importance of PrgL dimerization. Our findings provide insight into the molecular building blocks of Gram-positive T4SS, highlighting similarities but also unique features in PrgL compared to other VirB8-like proteins.

INTRODUCTION

Type 4 secretion systems (T4SS) are highly versatile molecular machines that are found in many bacterial species. This versatility is demonstrated by the fact that T4SSs take part in various functions such as (1) transfer of DNA from bacterial donor cells into recipient cells, (2) transfer of effector proteins into eukaryotic cells, (3) exchange DNA with the milieu, and (4) delivery of toxins to kill competing bacterial cells (Grohmann et al., 2018). Over the past decade our understanding of the structure and function of T4SSs has increased drastically, with biochemical studies coupled to crystallography and cryo-electron microscopy (both single particle and tomography) of T4SS model systems (Cascales et al., 2013; Hu et al., 2019a, 2019b; Low et al., 2014; Peña et al., 2012). However, all well studied systems to date are of Gram-negative origin. Although the overall composition and structure of Gram-positive T4SSs deviate from their Gram-negative counterparts, we know rather little of them. For the conjugative T4SSs, the DNA processing proteins and the ATPases that drive transport are thought to be similar. However, the makeup of the actual T4SS channel is completely different, owing to Gram-positives only having one membrane and a thick cell wall, compared to the Gram-negative double membrane and periplasmic space. These differences mean that structural features and domains that in the Gram-negative systems reside in the periplasmic space are located outside the cell in the Gram-positive T4SSs, where they reside within the thick cell wall.

Although the overall task of all conjugative T4SSs is the same, Gram-positive T4SSs have substantial differences in the channel composition and thus also in their structure and function compared with their Gram-negative counterparts, with only very limited structural data available (Goessweiner-Mohr et al., 2013a; Grohmann et al., 2018).

Since its discovery at the end of the 1970s, the conjugative plasmid pCF10 from *Enterococcus faecalis* has been serving as a model system for pheromone-regulated conjugation in Gram-positive bacteria (Dunny et al., 1978). The *pQ* promotor in pCF10 transcribes one large operon that contains, among other genes, all open reading frames for the entire T4SS (Dunny, 2013; Dunny and Berntsson, 2016). Previous research on components of this system has focused on the DNA processing proteins and the extracellular adhesion proteins (Bhatty et al., 2015; Chen et al., 2008; Li et al., 2012; Rehman et al., 2019; Schmitt et al., 2018, 2020). However, little information is currently available about the composition or architecture of the translocation channel. The current mechanistic model is that the accessory factor PcfF binds to the *oriT* of pCF10, where it then recruits the relaxase PcfG that nicks, unwinds, and covalently binds to the ssDNA (Rehman et al., 2019). This complex, called the relaxosome, is thought to recruit the T4 coupling protein PcfC, which initiates and provides energy for the DNA transfer through the translocation channel (Álvarez-Rodríguez et al., 2020; Chen et al., 2008). The translocation channel itself is suggested to consist of seven proteins (PrgD, -F, -H, -I, -K, -L, and PcfH),
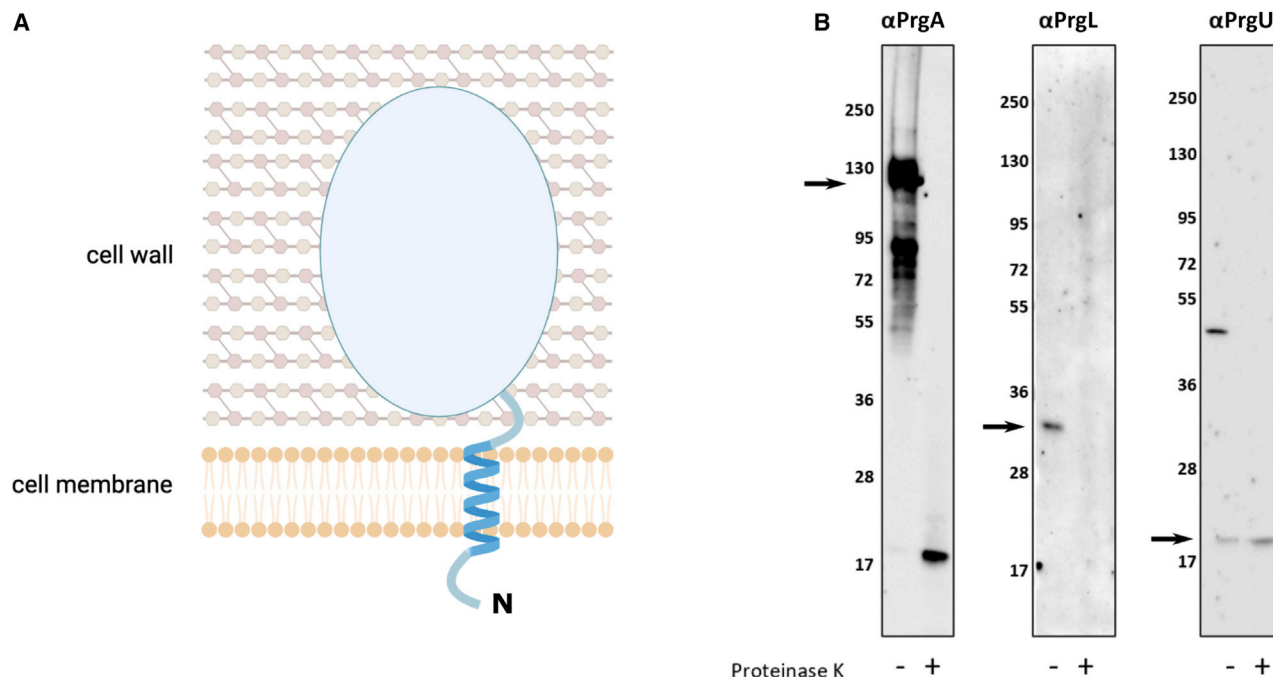
Figure 1. Cellular localization and topology of PrgL

(A) Schematic overview of PrgL, which has a short N-terminal stretch in the cytoplasm, a single transmembrane helix, and a short loop followed by its extracellular C-terminal domain (large gray circle, represents residues 52–208).

(B) Analysis of the topology of PrgA (extracellular control), PrgL and PrgU (intracellular control). Arrows indicate the correct band of the respective protein without any Proteinase K added. Samples were analyzed by western blotting using antibodies specific to PrgA, PrgL, and PrgU, with or without treatment with Proteinase K.

each containing at least one transmembrane-spanning helix (Alvarez-Martinez and Christie, 2009). These proteins are thought to form the membrane channel for export of the pCF10 transfer intermediate. However, no structural detail is available for any of these proteins, nor is the stoichiometry of these proteins in the channel known.

Two of the seven channel-forming proteins, PrgL and PrgD, have been predicted to be homologous to VirB8 in the Gram-negative *Agrobacterium tumefaciens* model system (Goessweiner-Mohr et al., 2013b). In the Gram-negative systems, VirB8 proteins contain a single transmembrane helix and a larger soluble domain that belongs to the superfamily of nuclear transport factor-2 (NTF2) domain, which is localized to the periplasmic space (Christie, 2016; Kumar and Das, 2001). VirB8 proteins are generally thought to form oligomers in the presence of their transmembrane domain, albeit examples exist of the NTF2-like domain oligomerizing on its own, such as the VirB8 homolog from the pKM101 system, TraE, which has been shown to form hexamers (Bourg et al., 2009; Casu et al., 2018; Fercher et al., 2016; Goessweiner-Mohr et al., 2013b). VirB8 homologs have in numerous cases been shown to be essential for the function of their T4SS and are suggested to play a role in complex assembly (Baron, 2006; Kumar et al., 2000; Sivanesan et al., 2010). However, even in the well-characterized Gram-negative systems, their structural roles have not yet been fully elucidated. Currently available structures of Gram-negative T4SSs complexes do not resolve VirB8 very well, and thus provide only very limited information on how VirB8 is part of the channel (Durie

et al., 2020; Kwak et al., 2017; Low et al., 2014; Sheedlo et al., 2020).

In this study, we present the crystal structure of the soluble NTF2-like domain of the VirB8 homolog PrgL from pCF10, and we show new data on the oligomeric state of the protein that also is imperative for its function *in vivo*. As so much is still unknown of Gram-positive T4SSs, the data presented here on PrgL provides important pieces of the puzzle in our understanding of these systems.

RESULTS

Topology analysis of PrgL

Full-length PrgL is predicted to be a membrane protein with a short N-terminal sequence followed by a single transmembrane (TM) helix and a C-terminal domain (Figure 1A). We utilized *Escherichia coli* and *Lactococcus lactis* as expression hosts for overproduction of PrgL and its soluble domain (PrgL$_{32-208}$). PrgL$_{32-208}$ (M_W = 22.5 kDa) was produced with a C-terminal 10× His-tag and purified with a yield of ca. 50 mg/L culture, and it was subsequently used to raise antibodies against PrgL. As VirB8-like proteins in Gram-negative T4SS have been shown to have their NTF2-like domain in the periplasmic space (Bailey et al., 2006; Goessweiner-Mohr et al., 2013b; Porter et al., 2012; Terradot et al., 2005), but one Gram-positive homolog has been indicated to have it in the cytoplasm (Fercher et al., 2016), we decided to investigate the topology of PrgL. We therefore analyzed PrgL expressed from the pCF10 plasmid in *E.*
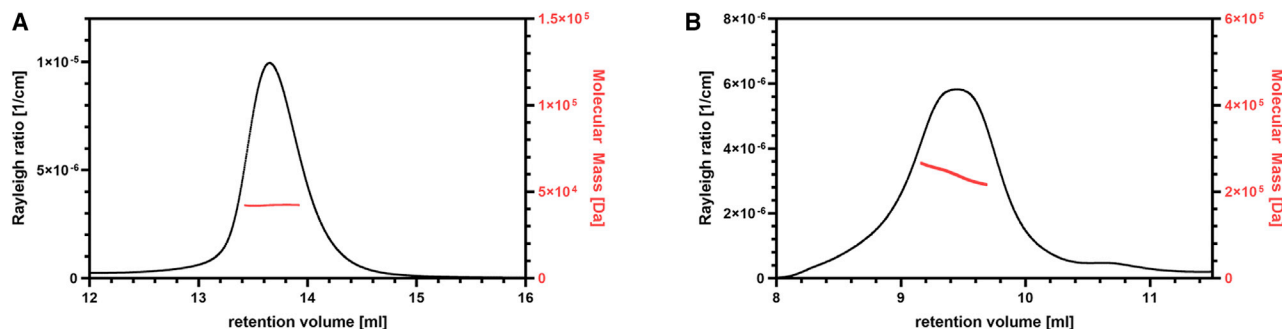
Figure 2. SEC-MALS of PrgL$_{32-208}$
The elution profile of PrgL$_{32-208}$ WT is shown with the average molecular mass of the dimer (A) and the higher order oligomer (B) calculated by MALS.

faecalis via a protease protection assay using Proteinase K, with two other pCF10 T4SS proteins as controls: PrgA and PrgU (Lassinantti et al., 2021; Schmitt et al., 2020) (Figure 1B). PrgA is an extracellular protein of the pCF10 T4SS involved in surface exclusion, which is anchored to the cell wall (Schmitt et al., 2020). PrgU is an intracellular protein that is involved in the transcriptional regulation of the pCF10 T4SS (Lassinantti et al., 2021). After addition of Proteinase K, the full-size bands of PrgA and PrgL (indicated by arrows in the figure) disappear, while PrgU remains intact. The same result is seen when performing the Proteinase K assay on *E. faecalis* cells complemented with PrgL (Figure S1). These experiments clearly show that PrgL has its NTF2-like domain on the outside of the cell.

PrgL forms both dimers and higher oligomers
As the yield of full-length PrgL proved difficult to scale up, we opted to determine the structure of the soluble domain of PrgL. Purified PrgL$_{32-208}$-His (M_W = 22.5 kDa) elutes as two separate peaks on SEC with the apparent masses of approximately 290 and 55 kDa (Figure S2), with the relative amount of the dodecamer increasing in a concentration-dependent manner. SEC-MALS analysis shows that the later elution peak corresponded to a molecular mass of 43.7 ± 0.4 kDa, which fits well with a dimeric form of PrgL$_{32-208}$. The earlier peak was not as homogenous and showed a larger variation in the calculated MW between runs but had an average mass of 250 ± 21.5 kDa, fitting with 10–12 copies of PrgL (Figure 2). To verify whether this higher order oligomer is formed by full-length PrgL-His (M_W = 26 kDa) *in vivo*, we characterized the complex formation by *in vivo* crosslinking after recombinant expression in *L. lactis*. After treatment with paraformaldehyde (PFA), full-length PrgL-His dimers and higher order oligomers were also observed on SDS-PAGE, with the largest complex migrating at the 250 kDa marker (Figure 3A). A similar oligomerization pattern is observed when performing *in vitro* crosslinking of the soluble domain of PrgL (Figure 3B), indicating that it is indeed the soluble domain that is the driving factor for oligomerization. The 250 kDa elution peak of purified PrgL$_{32-208}$-His was used for negative stain EM, but the particles were heterogeneous and the analysis did not provide any clear view of their structure. The SEC-MALS and crosslinking experiments show that both PrgL$_{32-208}$-His in solution and full-length PrgL-His *in vivo* form dimers and higher order oligomers. Our data show that the higher oligomer of PrgL

contains up to 12 subunits, suggesting that it could be a dodecamer, similar to the stoichiometry that was observed of the VirB8 protein in the R388 T4SS from *E. coli* (Low et al., 2014).

The structure of PrgL$_{32-208}$ reveals its dimerization interface
Obtaining high-quality cryo-EM grids with the PrgL$_{32-208}$ dodecamer unfortunately proved challenging, as the protein complexes consistently fell apart upon vitrification. Instead, we determined the structure of PrgL$_{32-208}$ via X-ray crystallography using fractions from the dimeric SEC peak. The initial phases were derived from single-wavelength anomalous dispersion (SAD) experiments using selenomethionine-substituted protein and the final structure was determined to a resolution of 1.7 Å (Table 1). The crystals belonged to the space group H3 and contained two molecules in the asymmetric unit. The final structural model corresponds to PrgL residues 52–189, as the N- and C-terminal ends were not visible in the electron density, likely due to them being flexible.

The overall structure of PrgL$_{32-208}$ consists of three antiparallel α-helices at the N-terminus and a highly curved β-sheet containing four antiparallel β-strands at the C-terminal end of the protein, which is wrapped around the first helix (Figures 4A–4B). The third helix is kinked, and there is a twist in the fourth β-strand formed by Pro^{167}. A pocket, formed by Tyr^{66}, Tyr^{67}, Lys^{69}, and Tyr^{132} lines a cavity in the center of the protein, which has a bis-Tris molecule (from the crystallization conditions) bound (Figures S3A and S3B).

A DALI search (Holm, 2020) with the structure of PrgL$_{32-208}$ confirms that PrgL is related to proteins from the VirB8 family, as it has the characteristic NTF2-like fold (Table S1). Compared to the archetypical VirB8 protein of *A. tumefaciens* (PDB: 2CC3) (Bailey et al., 2006), PrgL is missing an extended loop and short α-helix between β3 and β4. This was also found to be the case for other VirB8-like proteins from *E. faecalis*: TraH (PDB: 5AIW) and TraM (PDB: 4EC6) of the pIP501 plasmid (Fercher et al., 2016; Goessweiner-Mohr et al., 2013b) and from other Gram-positive bacteria like *Clostridium perfringens* (PDB: 3UB1) (Porter et al., 2012) (Figure 4C). PrgL$_{32-208}$ can be superimposed with the two other VirB8 family proteins of *E. faecalis*: TraH and TraM with an RMSD value of 2.4 Å and 2.8 Å, respectively (Table S1). Despite low sequence identity (12%–14%), two amino acids in the central pocket of PrgL (Tyr^{66} and Tyr^{67}) are
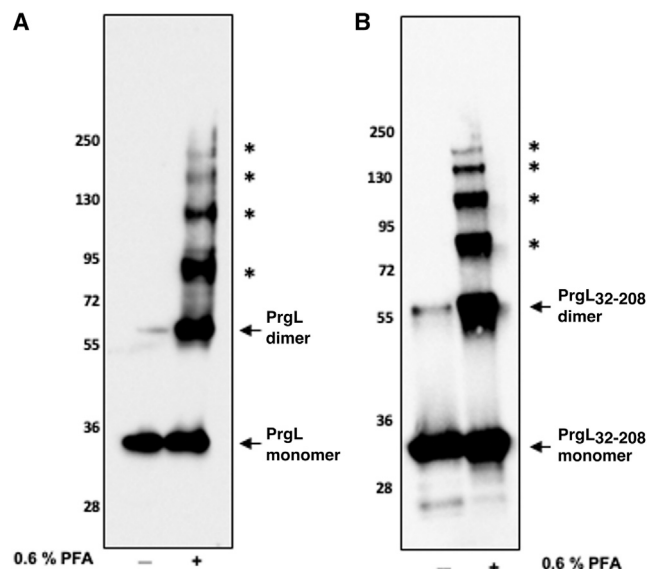
A
B

Figure 3. Analysis of the oligomerization state of PrgL

(A): *In vivo* crosslinking of *L. lactis* whole cells.

(B) *In vitro* crosslinking of purified PrgL$_{32-208}$. A final concentration of 0.6% formaldehyde (PFA) was used to crosslink the proteins. Higher molecular mass complexes of PrgL formed after crosslinking are indicated with an asterisk (*).

conserved in both TraH (Phe[70] and Tyr[71]) and TraM (Tyr[229] and Phe[230]) (Figure S3C).

The NTF2-like domains of various VirB8-like proteins have been shown to have numerous oligomeric states. For example, VirB8 from *A. tumefaciens* and TraE from pKM101 both form homodimers (Bailey et al., 2006; Casu et al., 2016), and TraH and TraM from pIP501 form monomers and trimers, respectively (Fercher et al., 2016; Goessweiner-Mohr et al., 2013b). In contrast to this, PrgL$_{32-208}$ forms both dimers and dodecamers in solution, as described earlier. Inspection of the PrgL$_{32-208}$ structure revealed that the PrgL dimer interface between the two monomers has a buried surface area of 910 Å^2, corresponding to ~10% of the total surface area of the monomer. The dimer interface is maintained by eight hydrogen bonds, one salt bridge, and a core hydrophobic patch that consists of residues Ile[127] and Leu[177] (Figure 4D). The solvation energy gain of the dimer interface is −5.9 kcal/mol, as calculated by PISA (Krissinel, 2015). To test if this hydrophobic interface indeed mediated dimer formation, we mutated Ile[127] to Glu. Purification of PrgL$_{32-208}$:I127E shows a marked shift to a later elution volume on SEC (Figure 5A), and SEC-MALS analysis showed that the peak fraction has a molecular mass of 26 ± 0.1 kDa, consistent with a monomeric state (Figure 5B). Besides a tailing void peak, indicating that PrgL$_{32-208}$:I127E is prone to aggregation, no defined dodecamer peak was observed on SEC (Figure S4). The dimer interface seen in the crystal structure thus corresponds to the actual dimer interface in solution. Comparing PrgL$_{32-208}$ with other structures of oligomeric NTF2-like domains reveals multiple different ways for these domains to oligomerize, with PrgL having a very different interface compared with VirB8 from *A. tumefaciens*, TraE from pKM101, or TraM from pIP501 (Figure 6). In fact, these four proteins all have different oligomerization interfaces.

Table 1. Data collection refinement statistics

Data collection summary	PrgL$_{32-208}$ SeMet	PrgL$_{32-208}$ native
Space group	H3	H3
Cell dimensions	–	–
a, b, c (Å)	124.5, 124.5, 66.4	124.5, 124.5, 66.4
Resolution (Å)	42.42–2.31 (2.39–2.31)	41.86–1.75 (1.79–1.75)
Completeness (%)	99.4 (94.3)	99.8 (96.3)
R$_{meas}$ (%)	38.8 (382)	4.9 (164)
I/σ (I)	7.9 (1.2)	16.3 (1.4)
CC(½)*	99.2 (28.9)	99.6 (50.3)
Redundancy	28.4 (18.2)	8.2 (7.8)
No. unique reflections	–	38,463 (3,733)
Refinement summary	–	–
Resolution (Å)	–	41.86–1.75 (1.79–1.75)
R$_{work}$ (%)	–	15.81
R$_{free}$ (%)	–	18.69
Number of atoms	–	–
Protein	–	2,202
Water	–	155
Other ligands	–	28
B-factors	–	–
Protein	–	46.64
Water	–	48.29
RMS deviations	–	–
Bond lengths (Å)	–	0.006
Bond angles (°)	–	0.76
Ramachandran statistics	–	–
Outliers (%)	–	0.00
Allowed (%)	–	0.76
Favored (%)	–	99.24

Oligomerization is required for *in vivo* function of PrgL

To test whether the dimerization of PrgL was important for the function of PrgL *in vivo*, we created an *E. faecalis prgL* knockout strain (OG1RF:pCF10Δ*prgL*), which we then complemented with either wild-type *prgL* or *prgL*:I127E. Deletion of *prgL* from pCF10 led to a more than 1000-fold reduction in conjugation efficiency but did not completely abrogate it (Figure 7). This phenotype could be fully rescued by complementing it with wild-type *prgL*. However, complementing with *prgL*:I127E, which showed similar levels of expression as the complemented wild-type *prgL* (Figure S5), only marginally restored the conjugation efficiency. These results show two things; (1) PrgL has a very important role in forming a functional T4SS, and (2) the ability of PrgL to oligomerize is imperative for its function. *In vivo* crosslinking of PrgL$_{I127E}$ in *E. faecalis* showed a similar crosslinking pattern as wild-type PrgL, indicating that higher oligomers could form despite the disrupted dimer (Figure S6).
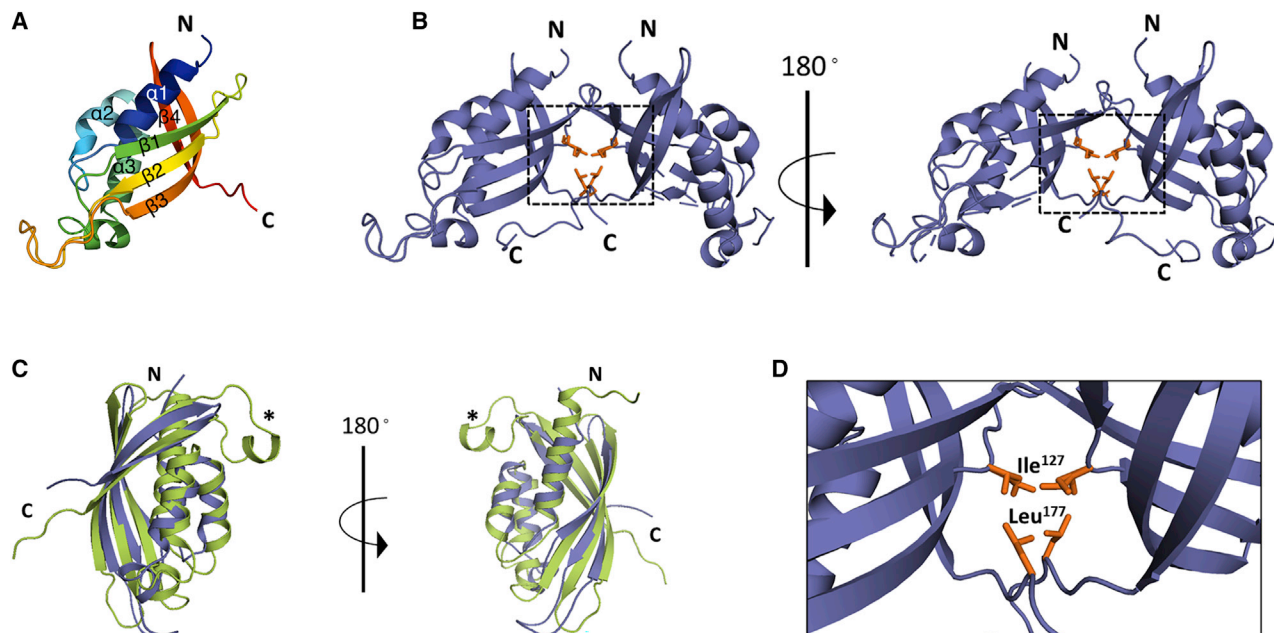
Figure 4. Crystal structure of PrgL$_{32-208}$ at 1.7-Å resolution
(A) Cartoon representation of a PrgL monomer, colored from the N-terminal (blue) to the C-terminal (red). α-Helices and β-strands are labeled.
(B) Cartoon representation with PrgL colored in blue, and residues involved in the dimerization colored in orange.
(C) Structural superimposition of PrgL$_{32-208}$ (blue) and VirB8 from *A. tumefaciens* (PDB: 2CC3, green). The extended loop with a short α-helix, found in nearly all VirB8-like proteins but absent in PrgL, is marked with an asterisk (*).
(D): Enlarged view of the box from (B), with the residues involved in dimerization highlighted in orange.

Interaction with other channel components

Since the Gram-positive T4SS channel assembly and the interaction between the different components remain unknown, we studied the interaction of PrgL with other components by *in vivo* crosslinking in *E. faecalis*. After inducing *E. faecalis* OG1RF:pCF10 cells with cCF10, cells were treated with PFA. Membrane fractions were prepared, loaded on SDS-PAGE, and further analyzed by western blot. Multiple bands could be detected with PrgL antibodies in the PFA cross-linked samples (Figure 8). Comparing these higher mass bands with the ones obtained after crosslinking recombinantly expressed PrgL in *L. lactis*, the same pattern of bands could be detected, migrating at roughly the same molecular masses (Figure S7). As the remaining T4SS machinery is absent in *L. lactis*, this indicates that PrgL does not strongly interact with other proteins of the T4SS or the *E. faecalis* membrane.

DISCUSSION

Type 4 secretion systems are a main driver of horizontal gene transfer, including the spread of antibiotic resistance genes between bacterial species (Alvarez-Martinez and Christie, 2009). One of the best characterized model systems is the VirB/D4 T4SS from *A. tumefaciens,* which has been studied since the 1970s (Christie and Cascales, 2005; Gurley et al., 1979; Li et al., 2019). Since their discovery, our understanding of these systems has deepened, and several T4SSs have now been structurally characterized (Bhatty et al., 2013; Hu et al., 2019a; Low et al., 2014). However, these characterized systems are all

of Gram-negative origin. There is only very limited biochemical or structural knowledge about T4SSs of Gram-positive origin, with the two systems that have been studied to some extent being the ones encoded on the pCF10 and pIP501 plasmids from *E. faecalis* (Kohler et al., 2018, 2019; Sterling et al., 2020).

In this study, we used structural and biochemical approaches to characterize PrgL, a component of the T4SS from the conjugative plasmid pCF10 of *E. faecalis*. PrgL was predicted to be a membrane protein with a short N-terminal sequence followed by a single transmembrane (TM) helix and a C-terminal domain. Despite very low sequence identity with other T4SS transfer proteins of the VirB8 family (Table S1), our results show that the overall structure of the soluble domain of PrgL (PrgL$_{32-208}$) is a VirB8 homolog with a nuclear transport factor-2 (NTF2)-like fold (Jakubowski et al., 2003) (Figure 4). VirB8-like proteins have, in other systems, been shown to be important for T4SS function, and they are thought to act as a scaffold for T4SS assembly (Baron, 2006; Kumar et al., 2000; Sivanesan et al., 2010). Here we could show that the absence of PrgL leads to a substantial decrease (more than three orders of magnitude) in conjugation efficiency *in vivo* (Figure 7). It is interesting to note that although PrgL is clearly very important for T4SS function and thus conjugation, in contrast to other homologs, it is not actually essential (Baron, 2006; Fercher et al., 2016). The reason for this is unclear but further emphasizes that important differences in these VirB8-like proteins exist between various systems.

According to the classification system for VirB8-like proteins, PrgL belongs to the ALPHA class of VirB8-like proteins (Goessweiner-Mohr et al., 2013b). For all classes it has been shown that
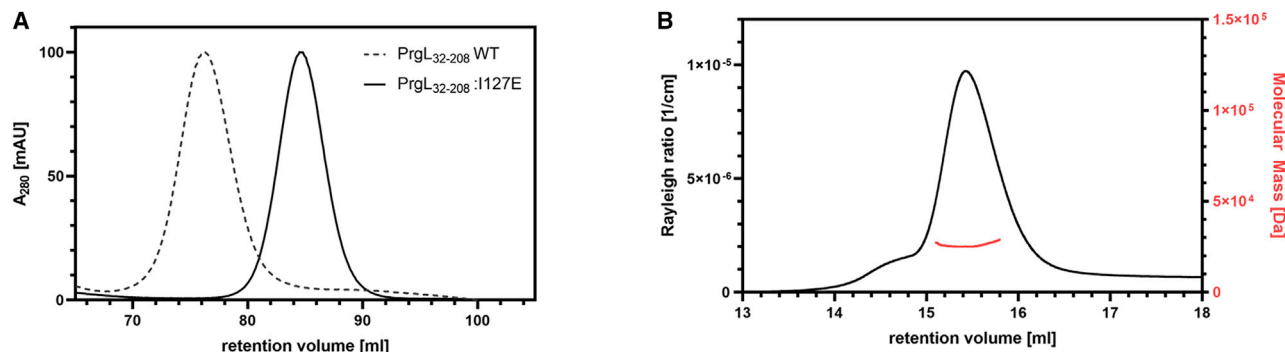
Figure 5. Elution profile of PrgL$_{32-208}$:I127E

(A) Elution profile of PrgL$_{32-208}$:I127E in comparison to PrgL$_{32-208}$ WT (dashed line) showing the later retention volume for the mutant.

(B) The elution profile of PrgL$_{32-208}$:I127E is shown with the average molecular mass calculated by MALS.

the NTF2-like domain resides outside the cell membrane, a characteristic that most Gram-negative and Gram-positive organisms seem to share (Bailey et al., 2006; Goessweiner-Mohr et al., 2013b; Porter et al., 2012; Terradot et al., 2005). The only described VirB8 homolog that deviates from this rule is TraH from the pIP501 plasmid, which has been proposed to have its NTF2-like domain in the cytoplasm (Fercher et al., 2016). Our Proteinase K experiments revealed that PrgL has its NTF2-like domain on the extracellular side (Figure 1), which is in line with its Gram-negative homologs. However, this of course means that the NTF2-like domain is situated outside the cell, in the environment of the cell wall, which raises the question of how this affects its function, something that has not yet been fully resolved.

VirB8-like proteins are known to oligomerize. A conserved NPXG motif, generally found on the extended loop between β3 and β4, is involved in the dimerization in nearly all VirB8 homologs described to date (Bailey et al., 2006; Gillespie et al., 2015; Terradot et al., 2005). As PrgL is missing this extended loop, this motif is not present. The pIP501 protein TraH also lacks this motif; instead, its oligomerization depends on its TM helix. We observed that oligomerization of PrgL occurs in absence of either the NPXG motif or the TM helix (Figure 2).

Comparing the oligomeric structures of various NTF2-like domains that are available reveals that these domains contain a high degree of plasticity with regard to how they oligomerize. VirB8 and TraE, both Gram-negative proteins, form dimers, but their dimerization interfaces are very different from each other. While both proteins share a sequence identity of 25% with an overall similar fold, the orientation of each monomer is different for these proteins, leading to altered amino acids involved in dimerization (Casu et al., 2016; Figures 6B and 6C). TraM in its turn forms trimers via a coiled-coil motif near the TM domain (Goessweiner-Mohr et al., 2013b; Figure 6D). With the coiled-coil motif missing in PrgL and its dimer showing an altered conformation compared to VirB8 and TraE, these results indicate that despite the overall similar fold of the domain, the different orientations of their dimers could have a biological significance. Inspection of the dimeric PrgL$_{32-208}$ structure revealed a hydrophobic pocket between the two monomers (Figure 4C). A single amino acid substitution in this pocket, isoleucine to glutamic acid, resulted in only monomeric PrgL$_{32-208}$ (Figure 5). Additionally, we could also show that this dimerization motif, which is different from all other characterized VirB8 homologs, was needed for T4SS function. Complementing a pCF10Δ*prgL* strain with *prgL*I127E only marginally
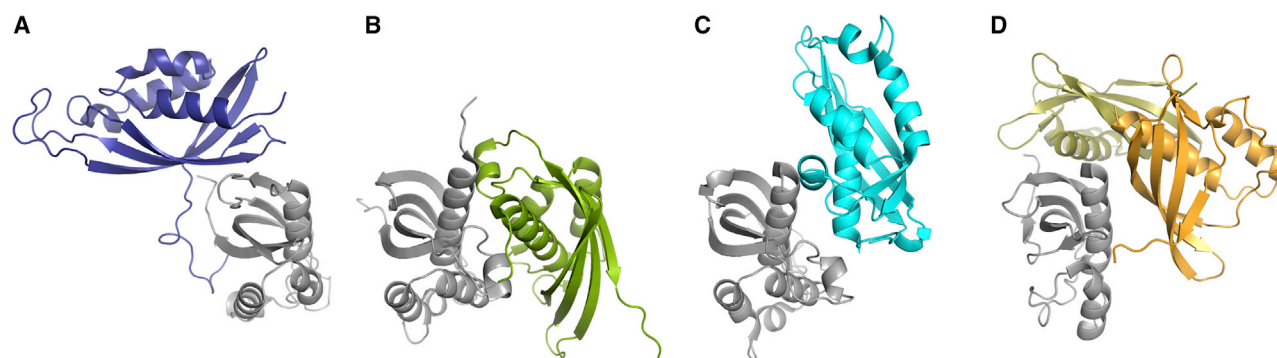

Figure 6. Comparison of oligomerization interfaces

(A) dimeric PrgL$_{32-208}$, (B) dimeric VirB8 from *A. tumefaciens*, PDB: 2CC3, (C) dimeric TraE from pKM101 PDB: 5I97, and (D) trimeric TraM from pIP501 PDB: 4EC6.

All structures have been superimposed on the subunit depicted in gray. Despite all these proteins having an NTF2-like domain fold, they all have very different oligomerization interfaces.
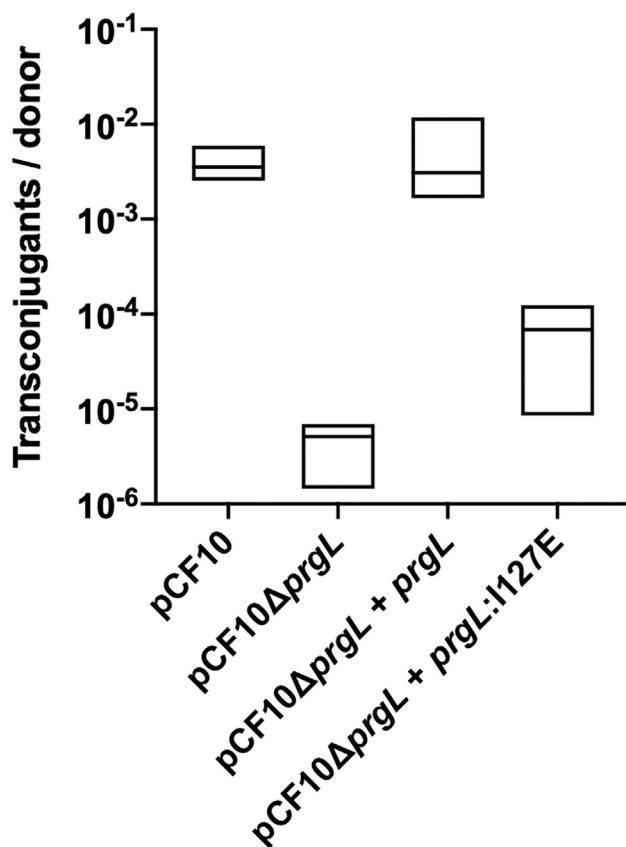
Figure 7. *In vivo* conjugation efficiency, comparing WT pCF10, pCF10Δ*prgL*, or pCF10Δ*prgL* complemented with wild-type *prgL* or pCF10Δ*prgL* complemented with *prgL*:I127E
Boxplot with the line showing the median value (N = 3).

restored the conjugation efficiency (Figure 7), clearly indicating that the ability of PrgL to dimerize is crucial for its function. While PrgL$_{I127E}$ could still form higher oligomers *in vivo*, only a monomer peak was observed when purifying it *in vitro*. Since PFA crosslinking is unsuitable for deducing interfaces, it is still an open question exactly how the PrgL dodecamer is built up.

While it is well known that VirB8-like proteins like to crystallize as dimers or trimers, higher order oligomers were only described *in vivo* and for full-length protein (Bailey et al., 2006; Fercher et al., 2016; Terradot et al., 2005). The only exception is the recently described OrfG, a VirB8 homolog from the Gram-positive *Streptococcus thermophilus* (Cappele et al., 2021). OrfG is shown to be able to form hexamers *in vitro*, albeit the equilibrium is heavily geared toward monomers (Cappele et al., 2021). PrgL on the other hand easily multimerizes *in vitro* by its NTF2-like domain alone, as shown by our SEC-MALS data. Furthermore, we could show that PrgL also forms these higher order oligomers *in vivo*. That PrgL can form dodecamers after recombinant expression *in vivo*, in the absence of other T4SS components, could indicate that it is one of the early structural building blocks of the T4SS, similar to what has been proposed for TraH in its cognate pIP501 T4SS (Fercher et al., 2016). Our *in vivo* crosslinking experiments on native pCF10 T4SS, expressed in *E. faecalis*,

do not indicate strong interactions between PrgL and the other components. This resonates with Gram-negative VirB8 proteins, where the working hypothesis is that the interactions with other channel components are of a transient nature. VirB8-like proteins have been shown to be involved in the binding of the transferred DNA, either directly or via their binding partners, such as the relaxases (Abajy et al., 2007; Cascales and Christie, 2004). Thus, it is possible that assembly of the T4SS machinery depends upon DNA binding and processing, something that is not tested in our experimental set up. Among the Gram-negative systems the VirB8 homolog from the pKM101 system has been shown to hexamerize. The R388 system is known to contain 12 copies of its VirB8 family protein, but whether these form an actual dodecamer, several smaller oligomers, or are part of other heteromeric oligomers is not yet known. Whether this dodecamer formation is unique to PrgL or is more widespread remains to be determined.

To conclude, our data shows that PrgL has a VirB8-like fold, validating previous bioinformatic studies (Bhatty et al., 2013; Goessweiner-Mohr et al., 2013b). In contrast to any previously described homolog, PrgL is shown to form higher oligomers, up to dodecamers, both *in vivo* via crosslinking experiments and *in vitro*. Importantly, this dodecameric formation occurs without aid of any NPXG motifs or its TM helix. *In vivo* conjugation experiments show that oligomerization is crucial for the function of PrgL. Furthermore, PrgL has its NTF2-like domain in the extracellular space, raising the question of how that could affect its function compared to its Gram-negative counterparts. Based on the available data of PrgL, and other VirB8 homologs, we speculate that PrgL is involved in the early stages of the assembly process of the translocation channel by acting as a scaffolding protein for the other T4SS components. The data presented here provides an important stepping stone for understanding Gram-positive T4SSs, an area in which we still know fairly little. Experiments to determine the exact nature of PrgL in the assembly of the T4SS and its interaction with other channel components remain exciting avenues for future research.

STAR★METHODS

Detailed methods are provided in the online version of this paper and include the following:

- KEY RESOURCES TABLE
- RESOURCE AVAILABILITY
  - Lead contact
  - Materials availability
  - Data and code availability
- EXPERIMENTAL MODEL AND SUBJECT DETAILS
- METHOD DETAILS
  - Bacterial strains and plasmids
  - Protein production and purification
  - Size exclusion chromatography coupled to multi-angle light scattering (SEC-MALS)
  - Crystallization and structure determination
  - *In vivo* conjugation
  - *In vivo* crosslinking
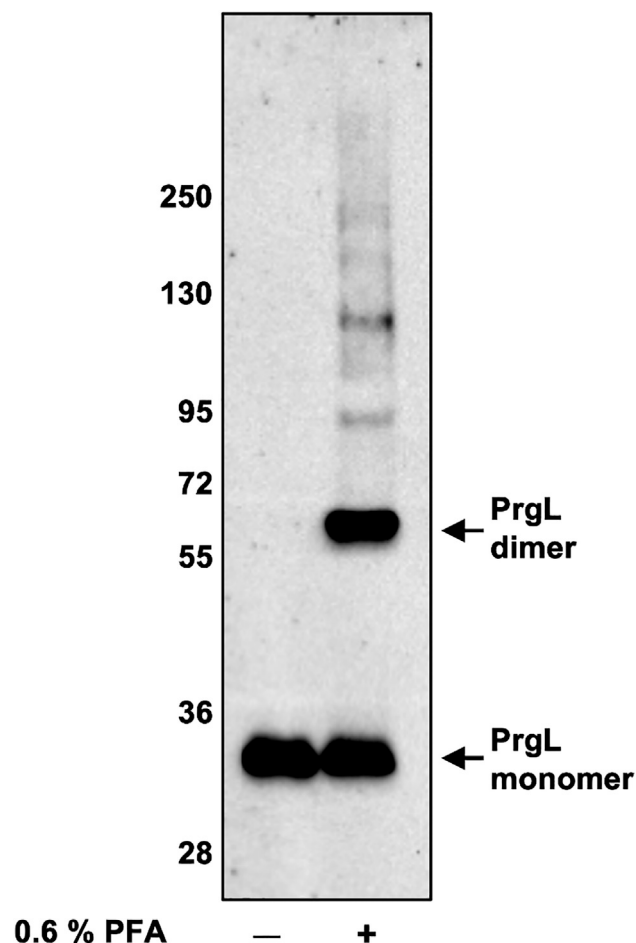 - Proteinase K digest
- QUANTIFICATION AND STATISTICAL ANALYSIS

Figure 8. *In vivo* analysis of potential interaction of PrgL with other components of the conjugation channel

Membrane fractions containing 5 μg of total protein were analyzed by western blotting after *in vivo* crosslinking of *E. faecalis* whole cells with a final concentration of 0.6% formaldehyde.

SUPPLEMENTAL INFORMATION

Supplemental information can be found online at https://doi.org/10.1016/j.str. 2022.03.013.

REFERENCES

Abajy, M.Y., Kopeć, J., Schiwon, K., Burzynski, M., Döring, M., Bohn, C., and Grohmann, E. (2007). A type IV-secretion-like system is required for conjugative DNA transport of broad-host-range plasmid pIP501 in gram-positive bacteria. J. Bacteriol. *189*, 2487–2496.

Adams, P.D., Grosse-Kunstleve, R.W., Hung, L.W., Ioerger, T.R., McCoy, A.J., Moriarty, N.W., Read, R.J., Sacchettini, J.C., Sauter, N.K., and Terwilliger, T.C. (2002). PHENIX: building new software for automated crystallographic structure determination. Acta Crystallogr. D Biol. Crystallogr. *58*, 1948–1954.

Alvarez-Martinez, C.E., and Christie, P.J. (2009). Biological diversity of prokaryotic type IV secretion systems. Microbiol. Mol. Biol. Rev. *73*, 775–808.

Álvarez-Rodríguez, I., Arana, L., Ugarte-Uribe, B., Gómez-Rubio, E., Martín-Santamaría, S., Garbisu, C., and Alkorta, I. (2020). Type IV coupling proteins as potential targets to control the dissemination of antibiotic resistance. Front. Mol. Biosci. *7*, 4068–4076.

Bae, T., Kozlowicz, B., and Dunny, G.M. (2002). Two targets in pCF10 DNA for PrgX binding: their role in production of Qa and prgX mRNA and in regulation of pheromone-inducible conjugation. J. Mol. Biol. *315*, 995–1007.

Bailey, S., Ward, D., Middleton, R., Grossmann, J.G., and Zambryski, P.C. (2006). Agrobacterium tumefaciens VirB8 structure reveals potential protein-protein interaction sites. Proc. Natl. Acad. Sci. U S A *103*, 2582–2587.

Baron, C. (2006). VirB8: a conserved type IV secretion system assembly factor and drug target. In Biochemistry and Cell Biology, pp. 890–899.

Bhatty, M., Camacho, M.I., González-Rivera, C., Frank, K.L., Dale, J.L., Manias, D.A., Dunny, G.M., and Christie, P.J. (2016). PrgU: a suppressor of sex pheromone toxicity in Enterococcus faecalis. Mol. Microbiol. *103*, 398–412.

Bhatty, M., Cruz, M.R., Frank, K.L., Gomez, J.A.L., Andrade, F., Garsin, D.A., Dunny, G.M., Kaplan, H.B., and Christie, P.J. (2015). Enterococcus faecalis pCF10-encoded surface proteins PrgA, PrgB (aggregation substance) and PrgC contribute to plasmid transfer, biofilm formation and virulence. Mol. Microbiol. *95*, 660–677.

Bhatty, M., Laverde Gomez, J.A., and Christie, P.J. (2013). The expanding bacterial type IV secretion lexicon. Res. Microbiol. *164*, 620–639.

Bourg, G., Sube, R., O'Callaghan, D., and Patey, G. (2009). Interactions between Brucella suis virb8 and its homolog Traj from the plasmid psb102 underline the dynamic nature of type IV secretion systems. J. Bacteriol. *191*, 2985–2992.

Cappele, J., Mohamad Ali, A., Leblond-Bourget, N., Mathiot, S., Dhalleine, T., Payot, S., Savko, M., Didierjean, C., Favier, F., and Douzi, B. (2021). Structural and biochemical analysis of OrfG: the VirB8-like component of the conjugative type IV secretion system of ICESt3 from Streptococcus thermophilus. Front. Mol. Biosci. *8*, 642606.

Cascales, E., and Christie, P.J. (2004). Definition of a bacterial type IV secretion pathway for a DNA substrate. Science *304*, 1170–1173.

Cascales, E., Atmakuri, K., Sarkar, M.K., and Christie, P.J. (2013). DNA substrate-induced activation of the Agrobacterium VirB/VirD4 type IV secretion system. J. Appl. Microbiol. *195*, 2691–2704.

Casu, B., Mary, C., Sverzhinsky, A., Fouillen, A., Nanci, A., and Baron, C. (2018). VirB8 homolog TraE from plasmid pKM101 forms a hexameric ring structure and interacts with the VirB6 homolog TraD. Proc. Natl. Acad. Sci. U S A *115*, 5950–5955.

Casu, B., Smart, J., Hancock, M.A., Smith, M., Sygusch, J., and Baron, C. (2016). Structural Analysis and inhibition of TraE from the pKM101 type IV secretion system. J. Biol. Chem. *291*, 23817–23829.

Chandler, J.R., Flynn, A.R., Bryan, E.M., and Dunny, G.M. (2005). Specific control of endogenous cCF10 pheromone by a conserved domain of the pCF10-encoded regulatory protein PrgY in Enterococcus faecalis. J. Appl. Microbiol. *187*, 4830–4843.

Chen, Y., Zhang, X., Manias, D., Yeo, H.-J., Dunny, G.M., and Christie, P.J. (2008). Enterococcus faecalis PcfC, a spatially localized substrate receptor for type IV secretion of the pCF10 transfer intermediate. J. Appl. Microbiol. *190*, 3632–3645.

Christie, P.J. (2016). The mosaic type IV secretion systems. EcoSal Plus *7*. https://doi.org/10.1128/ecosalplus.ESP-0020-2015.

Christie, P.J., and Cascales, E. (2005). Structural and dynamic properties of bacterial type IV secretion systems. Mol. Membr. Biol. *22*, 51–61.

de Ruyter, P., Kuipers, O.P., and de Vos, W.M. (1996). Controlled gene expression systems for Lactococcus lactis with the food-grade inducer nisin. Appl. Environ. Microbiol. *62*, 3662–3667.

Dunny, G., Funk, C., and Adsit, J. (1981). Direct stimulation of the transfer of antibiotic-resistance by sex-pheromones in streptococcus-faecalis. Plasmid *6*, 270–278.

Dunny, G.M. (2013). Enterococcal sex pheromones: signaling, social behavior, and evolution. Annu. Rev. Genet. *47*, 457–482.

Dunny, G.M., and Berntsson, R.P.-A. (2016). Enterococcal sex pheromones: evolutionary pathways to complex, two-signal systems. J. Bacteriol. *198*, 1556–1562.

Dunny, G.M., Brown, B.L., and Clewell, D.B. (1978). Induced cell aggregation and mating in Streptococcus faecalis: evidence for a bacterial sex pheromone. Proc. Natl. Acad. Sci. U S A *75*, 3479–3483.

Durie, C.L., Sheedlo, M.J., Chung, J.M., Byrne, B.G., Su, M., Knight, T., Swanson, M., Lacy, D.B., and Ohi, M.D. (2020). Structural analysis of the legionella pneumophila dot/icm type iv secretion system core complex. Elife *9*, 1–23.

Emsley, P., and Cowtan, K. (2004). Coot: model-building tools for molecular graphics. Acta Crystallogr. D Biol. Crystallogr. *60*, 2126–2132.

Emsley, P., Lohkamp, B., Scott, W.G., and Cowtan, K. (2010). Features and development of Coot. Acta Crystallogr. D Biol. Crystallogr. *66*, 486–501.

Fercher, C., Probst, I., Kohler, V., Goessweiner-Mohr, N., Arends, K., Grohmann, E., Zangger, K., Meyer, N.H., and Keller, W. (2016). VirB8-like protein TraH is crucial for DNA transfer in Enterococcus faecalis. Sci. Rep. *6*, 24643.

Geertsma, E.R. (2013). FX cloning: a versatile high-throughput cloning system for characterization of enzyme variants. Methods Mol. Biol. *978*, 133–148.

Geertsma, E.R. (2014). FX cloning: a simple and robust high-throughput cloning method for protein expression. Methods Mol. Biol. *1116*, 153–164.

Geertsma, E.R., and Dutzler, R. (2011). A versatile and efficient high-throughput cloning tool for structural biology. Biochemistry *50*, 3272–3278.

Geertsma, E.R., and Poolman, B. (2007). High-throughput cloning and expression in recalcitrant bacteria. Nat. Methods *4*, 705–707.

Gillespie, J.J., Phan, I.Q.H., Scheib, H., Subramanian, S., Edwards, T.E., Lehman, S.S., Piitulainen, H., Sayeedur Rahman, M., Rennoll-Bankert, K.E., Staker, B.L., et al. (2015). Structural insight into how bacteria prevent interference between multiple divergent type IV secretion systems. MBio *6*, e01867–15.

Goessweiner-Mohr, N., Arends, K., Keller, W., and Grohmann, E. (2013a). Conjugative type IV secretion systems in Gram-positive bacteria. Plasmid *70*, 289–302.

Goessweiner-Mohr, N., Grumet, L., Arends, K., Pavkov-Keller, T., Gruber, C.C., Gruber, K., Birner-Gruenberger, R., Kropec-Huebner, A., Huebner, J., Grohmann, E., et al. (2013b). The 2.5 A structure of the Enterococcus conjugation protein TraM resembles VirB8 type IV secretion proteins. J. Biol. Chem. *288*, 2018–2028.

Grohmann, E., Christie, P.J., Waksman, G., and Backert, S. (2018). Type IV secretion in gram-negative and gram-positive bacteria. Mol. Microbiol. *107*, 455–471.

Gurley, W.B., Kemp, J.D., Albert, M.J., Sutton, D.W., and Callis, J. (1979). Transcription of Ti plasmid-derived sequences in three octopine-type crown gall tumor lines. Proc. Natl. Acad. Sci. U S A *76*, 2828–2832.

Holm, L. (2020). DALI and the persistence of protein shape. Protein Sci. *29*, 128–140.

Hu, B., Khara, P., Song, L., Lin, A.S., Frick-Cheng, A.E., Harvey, M.L., Cover, T.L., and Christie, P.J. (2019a). In situ molecular architecture of the Helicobacter pylori cag type IV secretion system. MBio *10*, e00849–19.

Hu, B., Khara, P., and Christie, P.J. (2019b). Structural bases for F plasmid conjugation and F pilus biogenesis in Escherichia coli. Proc. Natl. Acad. Sci. U S A *116*, 14222–14227.

Jakubowski, S.J., Krishnamoorthy, V., and Christie, P.J. (2003). Agrobacterium tumefaciens VirB6 protein participates in formation of VirB7 and VirB9 complexes required for type IV secretion. J. Bacteriol. *185*, 2867–2878.

Kabsch, W. (2010). Xds. Acta Crystallogr. D Biol. Crystallogr. *66*, 125–132.

Kohler, V., Keller, W., and Grohmann, E. (2019). Regulation of gram-positive conjugation. Front. Microbiol. *10*, 1134.

Kohler, V., Vaishampayan, A., and Grohmann, E. (2018). Broad-host-range Inc18 plasmids: occurrence, spread and transfer mechanisms. Plasmid *99*, 11–21.

Krissinel, E. (2015). Stock-based detection of protein oligomeric states in jsPISA. Nucleic Acids Res. *43*, 314–319.

Kumar, R.B., and Das, A. (2001). Functional analysis of the Agrobacterium tumefaciens T-DNA transport pore protein VirB8. J. Bacteriol. *183*, 3636–3641.

Kumar, R.B., Xie, Y.H., and Das, A. (2000). Subcellular localization of the Agrobacterium tumefaciens T-DNA transport pore proteins: VirB8 is essential for the assembly of the transport pore. Mol. Microbiol. *36*, 608–617.

Kwak, M.-J., Kim, J.D., Kim, H., Kim, C., Bowman, J.W., Kim, S., Joo, K., Lee, J., Jin, K.S., Kim, Y.-G., et al. (2017). Architecture of the type IV coupling protein complex of Legionella pneumophila. Nat. Microbiol. *2*, 17114.

Langer, G., Cohen, S.X., Lamzin, V.S., and Perrakis, A. (2008). Automated macromolecular model building for X-ray crystallography using ARP/wARP version 7. Nat. Protoc. *3*, 1171–1179.

Lassinantti, L., Camacho, M.I., Erickson, R.J.B., Willett, J.L.E., De Lay, N.R., ter Beek, J., Dunny, G.M., Christie, P.J., and Berntsson, R.P.-A. (2021). Enterococcal PrgU provides additional regulation of pheromone-inducible conjugative plasmids. MSphere *6*, e00264–21.

Li, F., Alvarez-Martinez, C., Chen, Y., Choi, K.-J., Yeo, H.-J., and Christie, P.J. (2012). Enterococcus faecalis PrgJ, a VirB4-like ATPase, mediates pCF10 conjugative transfer through substrate binding. J. Appl. Microbiol. *194*, 4041–4051.

Li, Y.G., Hu, B., and Christie, P.J. (2019). Biological and structural diversity of type IV secretion systems. Microbiol. Spectr. *7*, 1–15.

Linares, D.M., Kok, J., and Poolman, B. (2010). Genome sequences of Lactococcus lactis MG1363 (revised) and NZ9000 and comparative physiological studies. J. Bacteriol. *192*, 5806–5812.

Low, H.H., Gubellini, F., Rivera-Calzada, A., Braun, N., Connery, S., Dujeancourt, A., Lu, F., Redzej, A., Fronzes, R., Orlova, E.V., et al. (2014). Structure of a type IV secretion system. Nature *508*, 550–553.

Panjikar, S., Parthasarathy, V., Lamzin, V.S., Weiss, M.S., and Tucker, P.A. (2005). Auto-Rickshaw: an automated crystal structure determination platform

as an efficient tool for the validation of an X-ray diffraction experiment. Acta Crystallogr. D Biol. Crystallogr. 61, 449–457.

Panjikar, S., Parthasarathy, V., Lamzin, V.S., Weiss, M.S., and Tucker, P.A. (2009). On the combination of molecular replacement and single-wavelength anomalous diffraction phasing for automated structure determination. Acta Crystallogr. D Biol. Crystallogr. 65, 1089–1097.

Peña, A., Matilla, I., Martín-Benito, J., Valpuesta, J.M., Carrascosa, J.L., De La Cruz, F., Cabezón, E., and Arechaga, I. (2012). The hexameric structure of a conjugative VirB4 protein ATPase provides new insights for a functional and phylogenetic relationship with DNA translocases. J. Biol. Chem. 287, 39925–39932.

Porter, C.J., Bantwal, R., Bannam, T.L., Rosado, C.J., Pearce, M.C., Adams, V., Lyras, D., Whisstock, J.C., and Rood, J.I. (2012). The conjugation protein TcpC from Clostridium perfringens is structurally related to the type IV secretion system protein VirB8 from Gram-negative bacteria. Mol. Microbiol. 83, 275–288.

Rehman, S., Li, Y.G., Schmitt, A., Lassinantti, L., Christie, P.J., and Berntsson, R.P.A. (2019). Enterococcal PcfF is a ribbon-helix-helix protein that recruits the relaxase PcfG through binding and bending of the oriT sequence. Front. Microbiol. 10, 1–11.

Schmitt, A., Hirt, H., Järvå, M.A., Sun, W.S., ter Beek, J., Dunny, G.M., and Berntsson, R.P.A. (2020). Enterococcal PrgA extends far outside the cell and provides surface exclusion to protect against unwanted conjugation. J. Mol. Biol. 432, 5681–5695.

Schmitt, A., Jiang, K., Camacho, M.I., Jonna, V.R., Hofer, A., Westerlund, F., Christie, P.J., and Berntsson, R.P.A. (2018). PrgB promotes aggregation, bio-film formation, and conjugation through DNA binding and compaction. Mol. Microbiol. 109, 291–305.

Sheedlo, M.J., Chung, J.M., Sawhney, N., Durie, C.L., Cover, T.L., Ohi, M.D., and Lacy, D.B. (2020). Cryo-EM reveals species-specific components within the Helicobacter pylori Cag type IV secretion system core complex. Elife 9, e59495.

Sivanesan, D., Hancock, M.A., Villamil Giraldo, A.M., and Baron, C. (2010). Quantitative analysis of VirB8-VirB9-VirB10 interactions provides a dynamic model of type IV secretion system core complex assembly. Biochemistry 49, 4483–4493.

Staddon, J.H., Bryan, E.M., Manias, D.A., Chen, Y., and Dunny, G.M. (2006). Genetic characterization of the conjugative DNA processing system of entero-coccal plasmid pCF10. Plasmid 56, 102–111.

Sterling, A.J., Snelling, W.J., Naughton, P.J., Ternan, N.G., and Dooley, J.S.G. (2020). Competent but complex communication: the phenomena of phero-mone-responsive plasmids. PLoS Pathog. 16, 1–19.

Terradot, L., Bayliss, R., Oomen, C., Leonard, G.A., Baron, C., and Waksman, G. (2005). Structures of two core subunits of the bacterial type IV secretion sys-tem, VirB8 from Brucella suis and ComB10 from Helicobacter pylori. Proc. Natl. Acad. Sci. U S A 102, 4596–4601.

Vanduyne, G.D., Standaert, R.F., Karplus, P.A., Schreiber, S.L., and Clardy, J. (1993). Atomic structures of the human immunophilin fkbp-12 complexes with Fk506 and rapamycin. J. Mol. Biol. 229, 105–124.

Vesić, D., and Kristich, C.J. (2013). A rex family transcriptional repressor influ-ences H2O2 accumulation by Enterococcus faecalis. J. Bacteriol. 195, 1815–1824.

STAR★METHODS

KEY RESOURCES TABLE

REAGENT or RESOURCE	SOURCE	IDENTIFIER
Bacterial strains		
List of strains in Table S2	N/A	N/A
Chemicals, Peptides and Recombinant Proteins		
Ampicillin/carbenicillin	Sigma	Cat#C1389
Kanamycin	Merk	Cat#K1377
Chloramphenicol	Sigma	Cat#C0378
Spectinomycin	Sigma	Cat#S4014
Erythromycin	Sigma	Cat#E5389
Brain-Heart Infusion broth	Sigma	Cat#53286
Tryptic soy broth without dextrose	Sigma	Cat# T3938
Yeast extract	Sigma	Cat# Y1625
Tetracycline	Sigma	Cat#87128
Fusidic acid	Sigma	Cat#F0881
X-Gal	VWR	Cat#MFCD00005666
SapI	Thermofisher scientific	Cat#ER1932
SfiI	Thermofisher scientific	Cat#ER1821
DpnI	Thermofisher scientific	Cat#ER1705
NcoI	Thermofisher scientific	Cat#FD0574
XbaI	Thermofisher scientific	Cat#FD0684
BamHI	Thermofisher scientific	Cat#FD0054
SalI	Thermofisher scientific	Cat#FD0644
Gistex	DSM Food Specialities	Cat#2463
KH_2PO_4/K_2HPO_4	VWR	Cat#26930.293/cat#26936.293
Glucose	VWR	Cat#101176K
Terrific Broth	Formedium	Cat#TBP0102
Glycerol	VWR	Cat#24388.320
IPTG	Sigma	Cat#I6758
L-Selenomethionine	AK scientific	Cat#M598
M9 minimal media	Formedium	Cat#MMS0102
Hepes	VWR	Cat#441485H
NaOH	VWR	Cat#28244.296
NaCl	VWR	Cat#85139.460
Imidazole	Sigma	Cat#I2399
Ni-NTA-Sepharose	Macherey Nagel	Cat#745400.100
LiCl	VWR	Cat#25009.236
TCEP	Sigma	Cat#646547
bis-Tris	VWR	Cat#0715
PEG 3350	Sigma	Cat#202444
Nisin	Sigma	Cat#N5764
paraformaldehyde	Sigma	Cat#P6148
4-Chloro-DL-phenylalanine	Sigma	Cat#C6506
Tris	VWR	Cat#0497
$MgSO_4$	VWR	Cat#25108.295
cCF10	JPT	N/A

(Continued on next page)

Continued

REAGENT or RESOURCE	SOURCE	IDENTIFIER
Sucrose	VWR	Cat#27480.294
$CaCl_2$	Fisher chemical	Cat#C/1400/60
Proteinase K	Roche	Cat#03115887001
10X EDTA free protease inhibitor	Roche	Cat#04693132001
Antibodies		
α-PrgL	Agrisera	N/A
α-PrgA	(Schmitt et al., 2020)	N/A
α-PrgU	(Bhatty et al., 2016)	N/A
Deposited Data		
Built model of PrgL	This paper	PDB: 7AED
VirB8 structure	Bailey et al. (2006)	PDB: 2CC3
TraH structure	Fercher et al. (2016)	PDB: 5AIW
TraM structure	Goessweiner-Mohr et al. (2013b)	PDB: 4EC6
TcpC structure	Porter et al. (2012)	PDB: 3UB1
TraE structure	Casu et al. (2016)	PDB: 5I97
Oligonucleotides		
List of oligonucleotides in Table S2	Eurofins	N/A
Recombinant DNA		
FXcloning vectors	(Geertsma and Dutzler, 2011) (Geertsma, 2013)	N/A
Software and Algorithms		
ASTRA	Wyatt Technology	https://store.wyatt.com/shop/viscostar/viscostar-iii/astra-software/
XDS	(Kabsch, 2010)	https://xds.mr.mpg.de
Auto-Rickshaw	(Panjikar et al., 2009)	https://www.embl-hamburg.de/Auto-Rickshaw/
ARP/wARP	(Langer et al., 2008)	https://www.embl-hamburg.de/ARP/
COOT	(Emsley et al., 2010)	https://www2.mrc-lmb.cam.ac.uk/personal/pemsley/coot/
PHENIX refine	(Adams et al., 2002)	https://phenix-online.org
PRISM	GraphPad Software	https://www.graphpad.com/scientific-software/prism/

RESOURCE AVAILABILITY

Lead contact
Further information and requests for resources and reagents should be directed to and will be fulfilled by the lead contact, Ronnie Berntsson (ronnie.berntsson@umu.se).

Materials availability
Wild-type or mutant expression plasmids are available upon request. This study did not generate new unique reagents.

Data and code availability
- All data generated or analyzed during this study are included in this published article and its supplemental information. All structural data has been deposited in the Protein Data Bank (PDB) and is publicly available. DOIs are listed in the key resources table.
- This paper does not report original code.
- Any additional information required to reanalyze the data reported in this paper is available from the lead contact upon request.

EXPERIMENTAL MODEL AND SUBJECT DETAILS

E. coli TOP10 was used for cloning. *L. lactis* NZ9000 was used for protein production (Linares et al., 2010), *E. faecalis* OG1RF was used as donor cells for *in vivo* studies (Dunny et al., 1981), and *E. faecalis* OG1ES was used as recipient cells (Staddon et al., 2006). Cells were grown and the protein purified as described in method details.

METHOD DETAILS

Bacterial strains and plasmids

For plasmids, strains and oligos used, please see Table S2. *E. coli* strain Top10 used for cloning, mutagenesis and plasmid amplification was cultured in Lysogeny broth (LB). Antibiotics were supplemented in LB when necessary, at the following concentrations: ampicillin (100 μg/mL), kanamycin (50 μg/mL), chloramphenicol (25 μg/mL), spectinomycin (50 μg/mL), and erythromycin (150 μg/mL). *E. faecalis* strains were cultured in Brain-Heart Infusion broth (BHI) or tryptic soy broth without dextrose (TSB-D) and supplemented with required antibiotics at the following concentrations: chloramphenicol (10 μg/mL), tetracycline (10 μg/mL), fusidic acid (25 μg/mL), erythromycin (20 μg/mL for chromosome-encoded resistance; 100 μg/mL for plasmid-encoded resistance), spectinomycin (250 μg/mL for chromosome-encoded resistance; 1000 μg/mL for plasmid-encoded resistance), streptomycin (1000 μg/mL).

Plasmids encoding *prgL* variants for expression in *E. coli* and *L. lactis* were designed using the FXcloning system (Geertsma, 2014). Briefly, the *prgL* gene variants were PCR amplified from pCF10 using the complementary primers: PrgL fw and PrgL rev for full-length PrgL or PrgL c-term fw and PrgL rev for PrgL$_{32-208}$, digested with SapI and cloned into the intermediate vector pINIT_kan. For expression in *L. lactis,* the pINIT_PrgL variant was sub-cloned into the pREXC3GH vector to generate a GFP and His-tagged variant while pINIT_PrgL$_{32-208}$ was sub-cloned into pREXC3H for a decahistidine-tagged variant of PrgL$_{32-208}$ and the resulting plasmids were transformed into *E. coli* TOP10 cells (Geertsma and Poolman, 2007). Subsequently, the *prgL* gene was transferred to pNZxLIC via SfiI digestion using the pSH71 harbouring vector pERL followed by transformation into *L. lactis* NZ9000. For expression in *E. coli* the PrgL$_{32-208}$ variant was ligated into the p7XC3H before being transformed into *E. coli* BL21 cells.

For generating PrgL$_{32-208}$:I127E, the pINIT_PrgL$_{32-208}$ plasmid was used as a template and PCR amplicon was amplified using site-directed mutagenesis primers PrgL I127E fw po and PrgL I127E rev po. Amplified products were digested with DpnI and subsequently transformed into *E. coli* strain TOP10. Further cloning for expression in *L. lactis* NZ9000 was followed after the same protocol as described above.

The *prgL*-expressing plasmids in *E. faecalis* were constructed by PCR amplifying the full-length *prgL* from pCF10 with the primer pair: NcoI-prgL-F and XbaI-prgL-R. The PCR product was digested by NcoI and XbaI and ligated into the same enzyme-treated pMSP3545S plasmid (Chandler et al., 2005). The ligation product was transformed into the *E. coli* strain TOP10 for subsequent plasmid isolation and DNA sequencing. The I127E mutation was then introduced into the *prgL*-expressing pMSP3545S plasmid mentioned above with the same mutagenesis strategy and primer pair as PrgL$_{32-208}$:I127E. The construction of *E. faecalis* OG1RF:pCF10Δ*prgL* strain was carried out with allelic exchange and counterselection aided by a pCJK218-derived plasmid (Vesić and Kristich, 2013), and the first and last 5 amino acids of PrgL were kept intact. In brief, the approximately 800-bp upstream region and 800-bp downstream region of *prgL* were PCR amplified with primer pairs of BamHI-prgL-UF-F and SalI-prgL-UF-R; SalI-prgL-DF-F and NcoI-prgL-DF-R respectively. The PCR products were digested with either BamHI/SalI or SalI/NcoI and ligated with BamHI/NcoI digested pCJK218. After plasmid isolation from the *E. coli* Top10 strain and DNA sequencing, the resulted construct was transformed into OG1RF:pCF10 via electroporation at 2 kV (Bae et al., 2002) with MicroPulser Electroporator (BioRad, U.S.A). The resulted *E. faecalis* transformant was then induced for allelic exchange by first enforcing plasmid integration to chromosome followed by excision. Plasmid integration was achieved by diluting overnight culture in fresh BHI medium (1:200) containing chloramphenicol and tetracycline, and incubating at 30°C for 2.5 h, then switching incubation temperature to 42°C for 2.5h before plating out on TSB-D agar plates with chloramphenicol, tetracycline, and X-Gal 250 (μg/mL). Positive colonies from PCR screening were subsequently induced for plasmid excision by culturing them in BHI with tetracycline at 30°C for several passages. Bacterial culture after passages was then plated on MM9YEG (1× M9, 0.25% yeast extract, 0.5% glucose, 1.5% agar) supplemented with 10 mM 4-Chloro-DL-phenylalanine, 250 μg/mL X-Gal, and tetracycline to select for white colonies in which no pCJK218 construct were carried. White colonies were then screened with PCR and sequencing (Vesić and Kristich, 2013).

Protein production and purification

PrgL variants were expressed as C-terminal decahistidine tagged proteins. For protein production in *L. lactis* NZ9000, cells were cultivated semianaerobically to an OD$_{600}$ = 1.0 in 2% Gistex (DSM Food Specialities B.V., Netherlands), 100 mM potassium phosphate (pH 7.0), 2.5% (w/v) glucose, and 5 μg/mL chloramphenicol at 30°C with gentle shaking before protein production was induced by adding 0.5% (v/v) of culture supernatant of the nisin A producing strain *L. lactis* NZ9700 (de Ruyter et al., 1996). Cells were pelleted 3 h after induction at 30°C, flash-frozen in liquid nitrogen and stored at - 20°C. For protein production of PrgL$_{32-208}$ in *E. coli* BL21(DE3), cells were cultivated aerobically at 37°C in TB medium supplemented with 0.4% (v/v) Glycerol to an OD$_{600}$ = 1.5, at which the temperature was lowered to 18°C and production of the protein was induced by adding 0.4 mM IPTG. Cells were pelleted 16 h after induction, flash-frozen in liquid nitrogen and stored at −20°C. Production of selenomethionine incorporated PrgL$_{32-208}$ was carried out in *E. coli* BL21(DE3) grown in M9 minimal medium supplemented with 50 mg/L L-Selenomethionine as described earlier (Vanduyne et al., 1993).

While full-length PrgL resides in the membrane, PrgL$_{32-208}$ is soluble and was purified from cytoplasmic extracts as follows: Cells were thawed and resuspended in Lysis Buffer 1 (20 mM HEPES/NaOH pH 7.8, 300 mM NaCl and 15 mM Imidazole pH 7.8). Cells were disrupted using a Constant cell disruptor (Constant Systems) by two or three passages at 25,000 psi or 39,000 psi when extracted from *E. coli* or *L. lactis*, respectively. Unbroken cells and cell debris were removed by centrifugation at 30,000 × g for 30 min. Proteins were purified at 4°C on Ni-NTA-Sepharose (Macherey-Nagel) packed in a gravity flow column. The column was washed with a total of 30 column volumes (CV) of Wash Buffer (20 mM HEPES/NaOH pH 7.8, 300 mM NaCl, 50 mM Imidazole pH 7.8) including a 10 CV washing step with Wash Buffer supplemented with 2 M LiCl before bound proteins were eluted with Elution Buffer (20 mM HEPES/NaOH pH 7.8, 300 mM NaCl, and 500 mM Imidazole pH 7.8). Subsequently, the proteins were further purified using a Hiload 16/600 Superdex 200 pg gelfiltration column (GE Healthcare) in SEC Buffer (20 mM HEPES/NaOH pH7.8 and 250 mM NaCl). Two peaks eluting at the molecular mass corresponding to a dodecamer and dimer were observed on gel filtration. Both peak fractions were handled separately in the following steps. The protein was concentrated using Amicon Ultra Centrifugal Filters (Merk Millipore). Selenomethionine derivated PrgL$_{32-208}$ was purified following the same protocol with the exception that 0.5 mM tris(2-carboxyethyl)-phosphine (TCEP) was added in all purification steps.

Size exclusion chromatography coupled to multi-angle light scattering (SEC-MALS)

Elution peaks corresponding to a molar mass of a dodecameric or dimeric protein of PrgL$_{32-208}$ were further analysed by SEC-MALS with the use of an ÄKTApure system (GE Healthcare) coupled to a miniDAWN TREOS II detector and an OptiLab T-rEX online refractive index detector (Wyatt Technology). The absolute molar mass was calculated by analysing the scattering data using the ASTRA analysis software package, version 7.2.2.10 (Wyatt Technology). BSA was used for calibration and proteins were separated on a Superdex 200 Increase 10/300 analytical SEC column (GE Healthcare) with a flow rate of 0.4 mL/min. The dimer (4 mg/mL) and do-decamer peaks (2 mg/mL) were injected with 400 and 200 μL, respectively, and eluted in 20 mM HEPES/NaOH (pH 7.8) and 250 mM NaCl. The refractive index increment of PrgL$_{32-208}$ was set at 0.185 mL/g and the extinction coefficient for UV detection at 280 nm was calculated from the primary structure of the protein construct.

Crystallization and structure determination

Native and selenomethionine derivatized PrgL$_{32-208}$ (in SEC buffer) were crystallized at 20°C by sitting drop vapor diffusion in 0.1 M bis-Tris (pH 5.5), 25% (w/v) PEG 3350 with a protein concentration of 6 mg/mL and a protein to reservoir ratio of 1:1. Crystals were flash-frozen in liquid nitrogen. X-ray diffraction data of native PrgL$_{32-208}$ crystals were collected at beamline BioMAX at the MAX IV Laboratory (Lund, Sweden). Diffraction data of selenomethionine derivatised PrgL$_{32-208}$ crystals were collected at beamline PX1 at the Swiss Light Source (SLS) (Paul Scherrer Institute, Switzerland). The data were processed using XDS (Kabsch, 2010). The crystallographic phase problem was solved by means of single-wavelength anomalous dispersion (SAD), the selenomethionine sites were found and refined by Auto-Rickshaw pipeline and an initial model built by ARP/wARP (Langer et al., 2008; Panjikar et al., 2005). The crystals belong to space group H3 and contained two molecules in the asymmetric unit. Building of the model was performed in COOT and refined at 1.8 Å using PHENIX refine to R$_{work}$ and R$_{free}$ values of 17.9% and 19.81%, respectively (Adams et al., 2002; Emsley and Cowtan, 2004). The structure has been deposited in the PDB code: 7AED).

In vivo conjugation

E. faecalis donor and recipient strains were inoculated in BHI with necessary antibiotics in overnight cultures. They were subsequently diluted in fresh BHI in a ratio of 1:10 without antibiotic and supplemented with 50 ng/mL nisin (Sigma) for those carrying the pMSP3545S plasmids to induce the expression from P$_{nis}$ and incubated at 37°C for 1h. The donor and recipient cells were then mixed at a ratio of 1:10 and stood at 37°C for 3.5 h in liquid for mating. The mating mixtures were serially diluted before plating out on selective BHI agar plates for either donor strains or transconjugants. The plasmid transfer frequencies were demonstrated as transconjugants cells per donor cell. Experiments were repeated three times in triplicate.

In vivo crosslinking

For formaldehyde crosslinking in *L. lactis* NZ9000 full-length PrgL was produced in 1L of media as described above. 3h after induction 50 mL of the culture was harvested and cells resuspended in 5 mL 1 × PBS before being divided into two equal aliquots. Formaldehyde was added to one sample to a final concentration of 0.6% while the second sample was kept untreated as negative control. Both samples were incubated at room temperature for 30 min before the reaction was quenched by addition of Tris/HCl (pH 8.0) to a final concentration of 100 mM. Cells were pelleted by centrifugation for 10 min at 3000 × g, resuspended in 20 mL Lysis buffer (50 mM potassium phosphate, pH 7.0, 10% glycerol, 1 mM MgSO$_4$) and treated as described above to acquire the isolated membrane fractions. Membranes were resuspended in 100 μL membrane buffer (50 mM potassium phosphate, pH 7.0, 10% glycerol) prior to loading on SDS-PAGE and subsequent immunological detection of PrgL by Western Blotting with an anti-PrgL antiserum (1:10,000 dilution). Note that the migration pattern of PrgL is dependent on the type of gel used. When using home-cast gels (Serva Electrophoreses) the PrgL monomer migrates close to its expected molecular weight of 26 kDa but when using pre-cast gradient gels (Expedeon) the apparent molecular weight is shifted to ca 33 kDa (compare Figures S5 and S6).

For interaction studies of PrgL with other proteins of the T4SS, *E. faecalis* strain OG1RF harboring the pCF10 plasmid was cultivated in BHI media containing 10 μg/mL Tetracycline at 37°C with gentle shaking to an OD$_{600}$ = 0.6–0.8 before induction with 5 ng/mL cCF10. Cells were pelleted after 1h statical incubation at 37°C, washed in 50 mL one × PBS, pelleted again and

subsequently resuspended in 6 mL crosslinking buffer (50 mM potassium phosphate, pH 7.0; 200 mM KCl; 250 mM Sucrose; 1 mM EDTA). One sample was incubated with PFA to a final concentration of 0.6%, while the other sample was kept untreated as negative control. Both samples were incubated at room temperature for 30 min before the reaction was quenched by addition of Tris/HCl (pH 8.0) to a final concentration of 100 mM. After a quenching time of 15 min samples were diluted with Lysis buffer (50 mM potassium phosphate, 10% glycerol, 1 mM $MgSO_4$) to a total volume of 30 mL and treated as described for the purification of full-length PrgL to acquire the isolated membrane fractions. The membranes were resuspended in 200 μL of membrane buffer (50 mM potassium phosphate, pH 7.0, 10% glycerol) prior to loading on SDS-PAGE and subsequent immunological detection of PrgL by Western Blotting with an anti-PrgL antiserum (1:10,000 dilution).

Proteinase K digest

For proteinase K assays *E. faecalis* OG1RF:pCF10 cells were grown and induced as described for the *in vivo* crosslinking. After harvesting 1L of induced culture, cells were washed in 20 mL proteinase-buffer (30 mM Tris/HCl pH 7.5, 500 mM Sucrose, 10 mM $CaCl_2$), pelleted for 20 min at 3200 × g, resuspended in 18 mL proteinase-buffer and divided into six equal aliquots à 3 mL before being flash-frozen and stored at - 80°C. For the proteinase K assay 3 mL of cells were thawed and aliquoted into 950 μL samples. Proteinase K digest was started by adding proteinase K to all samples with a final concentration of 50 μg/mL and incubating them for 10 min at 30°C. The reaction was stopped by adding 100μL of 10× EDTA free protease inhibitor and incubated 15 min at room temperature prior to the immunological detection of PrgA, PrgL, and PrgU by Western Blotting with anti-PrgA (1:10,000 dilution), anti-PrgL or anti-PrgU antiserums (1:5 000 dilution).

QUANTIFICATION AND STATISTICAL ANALYSIS

Conjugation assay, visualized in Figure 7, was conducted with three independent experiments (n = 3) in triplicate as mentioned in method details, with the error reported being the standard deviation. Prism 9.0 was used for the statistical analysis.